The Abdus Salam
International Centre for Theoretical Physics

United Nations
Educational, Scientific and
Cultural Organization

IAEA
International Atomic Energy Agency

2052-60

Summer College on Plasma Physics

10 - 28 August 2009

Simulation and modeling of nonlinear mirror modes

Thierry Passot
Observatoire de la Côte d'Azur
France

Simulation and modeling of nonlinear mirror modes

T. Passot, P.L. Sulem
CNRS, Observatoire de la Côte d'Azur, Nice

P. Hellinger, P. Travnicek
Institute of Atmospheric Physics, Prague

E. Kuznetsov
Lebedev Physical Institute and
Space Research Institute, Moscow

F. Califano
Dipartimento di Fisica, Universita' di Pisa

International Symposium on Cutting Edge Plasma Physics, *Trieste, 24-28 August 2009*

Outline

1. Satellite observations

2. Numerical simulations of the Vlasov-Maxwell equations

3. Modeling the structure formation in a large domain
    - Asymptotic expansion near a Maxwellian distribution
    - Coupling with quasi-linear diffusion equation
    - Properties and simulations of the model equation

4. The case of small domains (presence of trapping)

5. Summary

1. Satellite observations

Magnetic structures (**humps** or **holes**)
that are quasi-stationary in the plasma frame,
with **no or little change in the magnetic field direction** are commonly observed in the
solar wind and the planetary magnetosheaths.

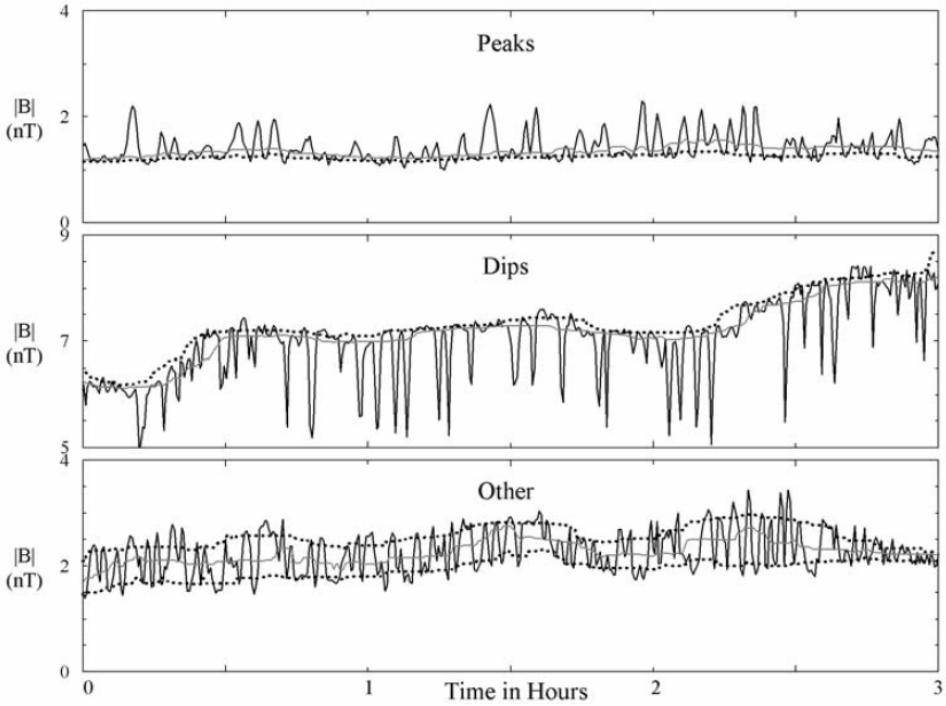

Figure 1. Each panel shows 3 hours of Galileo magnetometer field magnitude data (solid black line), appropriate quartiles (dotted), and the median value (solid gray) computed using 20 min sliding windows with single sample shifts. The panels show examples of "peaks" (top), "dips" (middle), and "other" (bottom) structures.

Joy et al. J. Geophys. Res. **111**, A12212 (2006)

Structures observed in the Jovian magnetosheath

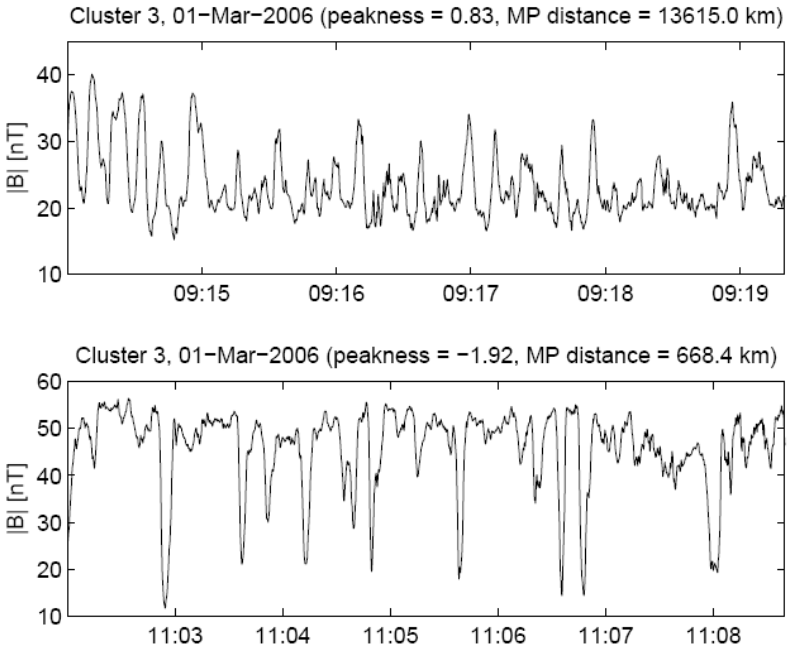

Figure 1. An example of mirror mode structures of the two types. Top panel: peaks (peakness = 0.83), bottom panel: dips (peakness = -1.92).

Soucek, Lucek & Dandouras JGR **113**, A04203 (2008)

Structures observed in
the terrestrial magnetosheath

Usually viewed as **nonlinear mirror modes**

Main properties of observed structures:

- Structures are quasi-static in the plasma frame (propagating drift mirror modes exist in density gradients)
- Small change in the magnetic field direction
- Observed in regions displaying: ion temperature anisotropy $T_{i\perp} > T_{i\parallel}$
  β of a few units
  (conditions met under the effect of plasma compression in front of the magnetopause).
  Not always in a mirror unstable regime.
- Magnetic fluctuations mostly affect the parallel component.
- Cigar-like structures, quasi-parallel to the ambient field, with a transverse scale of a few Larmor radii.
- Density is anticorrelated with magnetic field amplitude.

Origin of these structures is still not fully understood.

Usually viewed as nonlinearly saturated states of the mirror instability,
or possibly, in particular in the solar wind, remnants of mirror structures
created upstream of the point of observation (Winterhalter et al. 1995).

Other recent interpretations:

- trains of slow-mode magnetosonic solitons (Stasiewicz 2004)
- mirror instability is the trigger, generating high amplitude fluctuations that evolve such as to become nonlinear solutions of isotropic or anisotropic plasma equations (Baumgärtel, Sauer & Dubinin 2005)

Linear instability

cold electrons, $f = f(v_\parallel^2, v_\perp)$

Venedov and Sagdeev (1958), Chandrasekhar et al. (1958), Hasegawa (1969), Hall (1979), Gary (1992), McKean et al. (1992,1994), Southwood and Kivelson (1993), Pantellini & Schwartz 1995, Pokhotelov et al. (2005 and references therein), Hellinger (2007).

Instability condition: $\Gamma = \beta_\Gamma - \beta_\perp - 1 > 0$ (Shapiro & Shevchenko 1964)

$$\beta_\perp = \frac{mn}{p_B}\int \frac{v_\perp^2}{2} f d^3v \qquad \beta_\parallel = \frac{mn}{p_B}\int v_\parallel^2 f d^3v \qquad \beta_\Gamma = -\frac{mn}{p_B}\int \frac{v_\perp^4}{4}\frac{\partial f}{\partial v_\parallel^2} d^3v$$

n is the background density of the protons, m their mass

$p_B = B_0^2/8\pi$ background magnetic pressure

Linear growth rate (near threshold):

$$\gamma_{\boldsymbol{k}} = \sqrt{\frac{2}{\pi}}|k_\parallel|\tilde{v}\left(\Gamma - \frac{3}{2}\tilde{r}^2 k_\perp^2 - \frac{k_\parallel^2}{k_\perp^2}\chi\right)$$

$$\tilde{v}^{-1} = -\sqrt{2\pi}\frac{mn}{p_B}\int \frac{v_\perp^4}{4}\delta(v_\parallel)\frac{\partial f}{\partial v_\parallel^2} d^3v$$

$$\chi = 1 + \frac{1}{2}(\beta_\perp - \beta_\parallel)$$

$$\tilde{r}^2 = -\frac{mn}{24 p_B}\frac{1}{\Omega^2}\int \left(v_\perp^6 \frac{\partial f}{\partial v_\parallel^2} + 3v_\perp^4 f\right) d^3v$$

For a bi-Maxwellian distribution:

$$\beta_\perp = mnv_{th\perp}^2/p_B$$
$$\beta_\parallel = mnv_{th\parallel}^2/p_B$$
$$\tilde{v} = v_{th\parallel}/\beta_\Gamma$$
$$\beta_\Gamma = \beta_\perp^2/\beta_\parallel$$
$$\tilde{r} = v_{th\perp}(\beta_\Gamma - \beta_\perp)^{1/2}/\Omega$$

Instability condition:

$$\Gamma^* \equiv \beta_\perp\left(\frac{\beta_\perp}{\beta_\parallel} - 1\right) - 1 > 0$$

Growth rate:

$$\gamma_{\boldsymbol{k}} = |k_z| v_{\mathrm{th}\parallel}\frac{\beta_\parallel}{\sqrt{\pi}\beta_\perp}\left[\frac{\beta_\perp}{\beta_\parallel} - 1 - \frac{1}{\beta_\perp} - \frac{k_z^2}{k_\perp^2\beta_\perp}\left(1 + \frac{\beta_\perp - \beta_\parallel}{2}\right) - \frac{3}{4\beta_\perp}k_\perp^2\rho_L^2\right]$$

(ρ_L: ion Larmor radius)

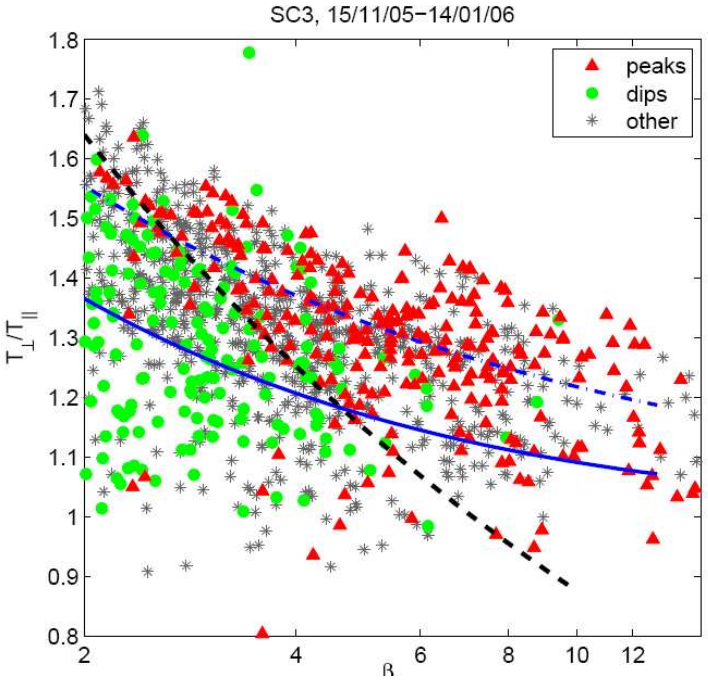

Figure 3. Distribution of mirror modes of different types in the anisotropy-beta plane. Red triangles denote peaks with $\mathcal{P} > 0.3$, green squares dips ($\mathcal{P} < -0.6$) and the remaining ambiguous mirror mode events are marked by grey stars.

Soucek, Lucek & Dandouras, JGR **113**, A04203 (2008)

Solid blue line: theoretical (bi-Maxwellian) mirror threshold

$$\frac{T_\perp}{T_{||}} > 1 + 1/\beta_\perp$$

Dashed-dotted blue line: empirical marginal stability

$$\frac{T_\perp}{T_{||}} = 1 + \frac{a}{\beta_{||}^b} \qquad \begin{array}{l} a = 0.83 \\ b = 0.58 \end{array}$$

Black dashed line: fitted boundary between peaks and dips

$$\frac{T_\perp}{T_{||}} = \frac{2.15}{\beta_{||}^{0.39}}$$

"Peaks are typically observed in an unstable plasma, while mirror structures observed deep within the stable region appear almost exclusively as dips".

Solar wind: "Although the plasma surrounding the holes was generally stable against the mirror instability, there are indications that the *holes may have been remnants of mirror mode structures* created upstream of the points of observation" (Winterhalter et al. 1995).

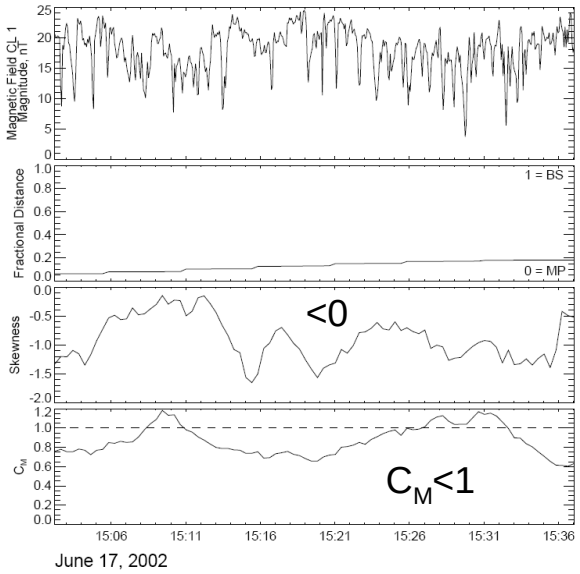

Skewness

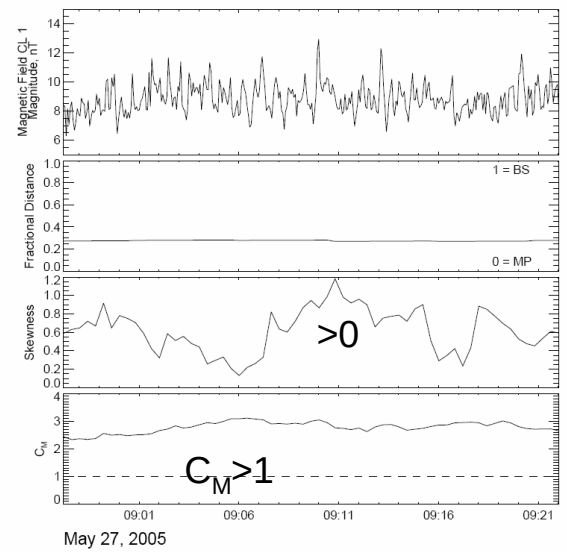

C_M <1 : subcritical
C_M >1 : supercritical
(for bi-Maxwellian equilibrium)

Magnetic holes: mostly in subcritical regime

Magnetic humps: in supercritical regime

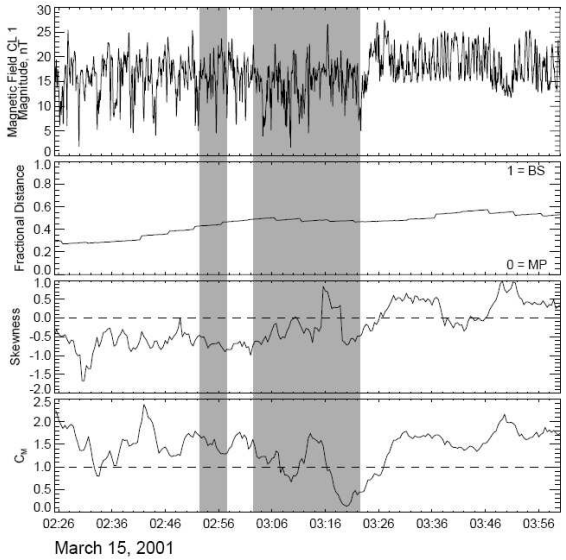

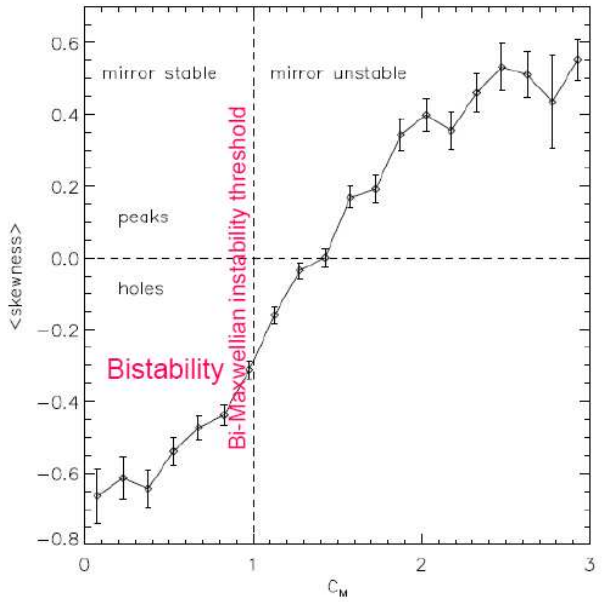

$$C_M = \beta_{p\perp}\left(\frac{T_{p\perp}}{T_{p\parallel}} - 1\right)$$

Génot et al., Ann. Geophys. **27,** 601 (2009).

2. Numerical simulations of the Vlasov-Maxwell equations

Shed light on the time evolution and on the origin of the structures.

Mirror unstable regime near threshold in a large domain

1D simulation: $\theta_{kB} = 72.8°$ (most unstable direction)

$\beta_{p\parallel} = 1 \; \beta_{p\perp} = 1.857 \quad \beta_e = 10^{-2}$

With a PIC code in a large domain:

Domain size= 2048 c/ωpi

Growth rate: 0.005 Ωp

1024 cells with 500 000 particles/cell

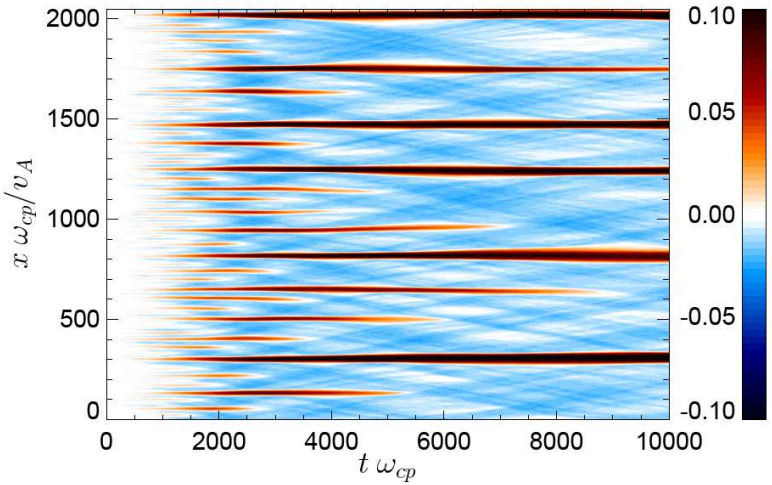

Color plot of the fluctuations of the magnetic field component B_η perpendicular to the direction ζ of spatial variation, as a function of ζ and t.

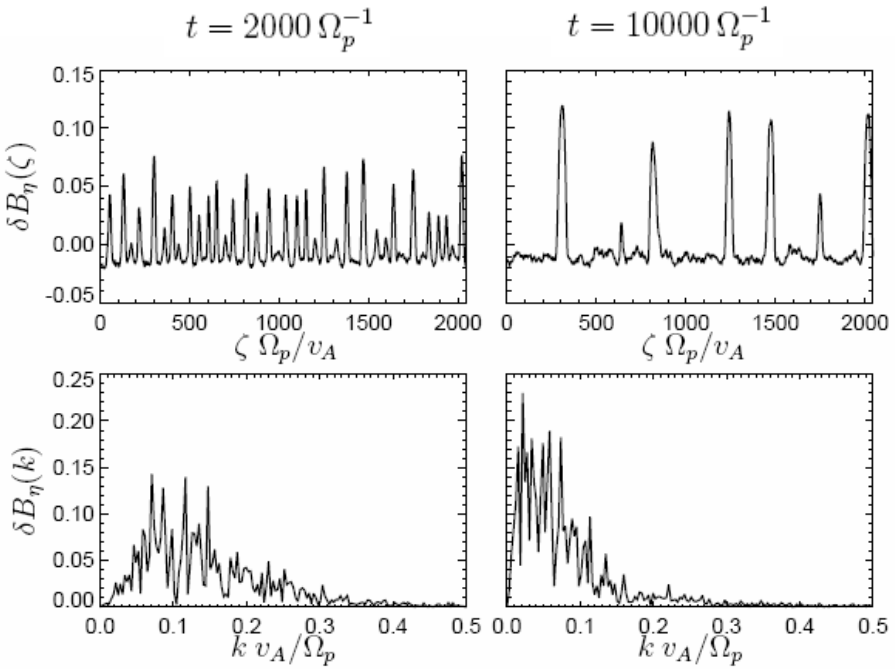

A large number of modes are excited.

Humps form and undergo coarsening.

First mechanism suggested for saturation: based on **quasi-linear theory** (Shapiro & Shevchenko 1963)

- Assumes space homogeneity (thus absence of coherent structures); can thus be valid at early times only.
- Requires many modes in interaction, thus an extended domain.
- Mainly associated with a diffusion process in velocity space (dominantly along the ambient field).

$$\frac{\partial f}{\partial t} = \frac{\partial}{\partial v_\parallel} D_{\parallel\parallel} \frac{\partial f}{\partial v_\parallel} + \frac{1}{v_\perp} \frac{\partial}{\partial v_\perp} v_\perp \left(D_{\perp\parallel} \frac{\partial f}{\partial v_\parallel} + D_{\perp\perp} \frac{\partial f}{\partial v_\perp} \right)$$

$$D_{\parallel\parallel} = v_\perp^4 \sum_{\boldsymbol{k}} \frac{|b_{\boldsymbol{k}}|^2}{4} \frac{\gamma_{\boldsymbol{k}} k_\parallel^2}{k_\parallel^2 v_\parallel^2 + \gamma_{\boldsymbol{k}}^2}$$

$$D_{\perp\parallel} = -2 \frac{v_\parallel}{v_\perp} D_{\parallel\parallel}$$

$$D_{\perp\perp} = v_\perp^2 \sum_{\boldsymbol{k}} \gamma_{\boldsymbol{k}} \frac{|b_{\boldsymbol{k}}|^2}{4}$$

$$b_{\boldsymbol{k}} = \delta B_z(\boldsymbol{k}) / B_0$$

$$\frac{\partial b_{\boldsymbol{k}}}{\partial t} = \gamma_{\boldsymbol{k}} b_{\boldsymbol{k}}$$

linear growth rate

Hellinger & al., GRL, 36, L06103, (2009)

fluctuating magnetic energy

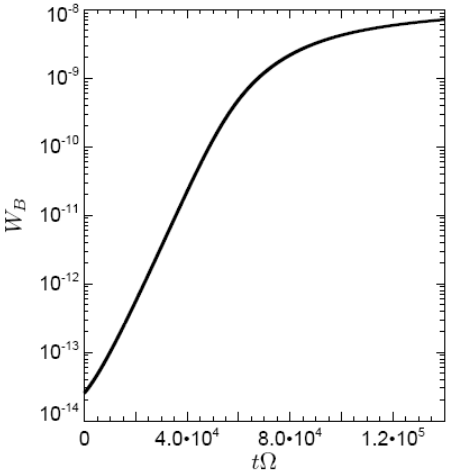

distance from threshold

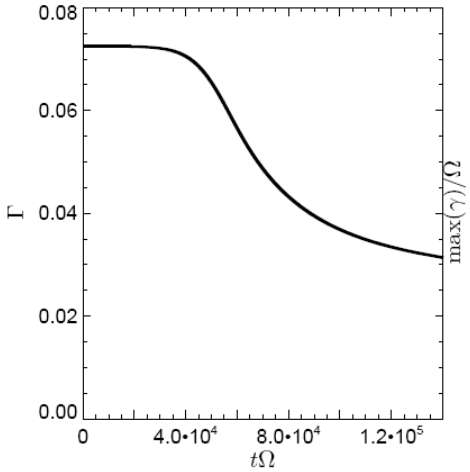

maximum growth rate

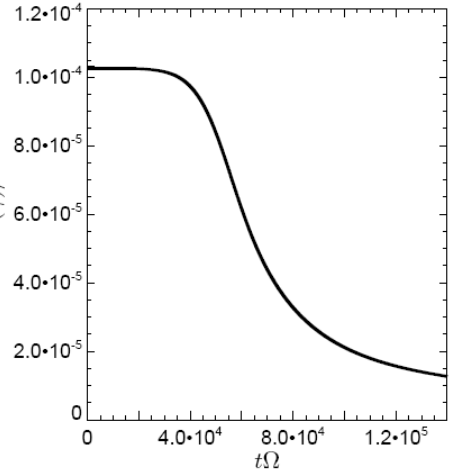

Perturbation of the space-averaged distribution function $\Delta f = f - f^{(0)}$

QL theory

t= 1.4 10^5

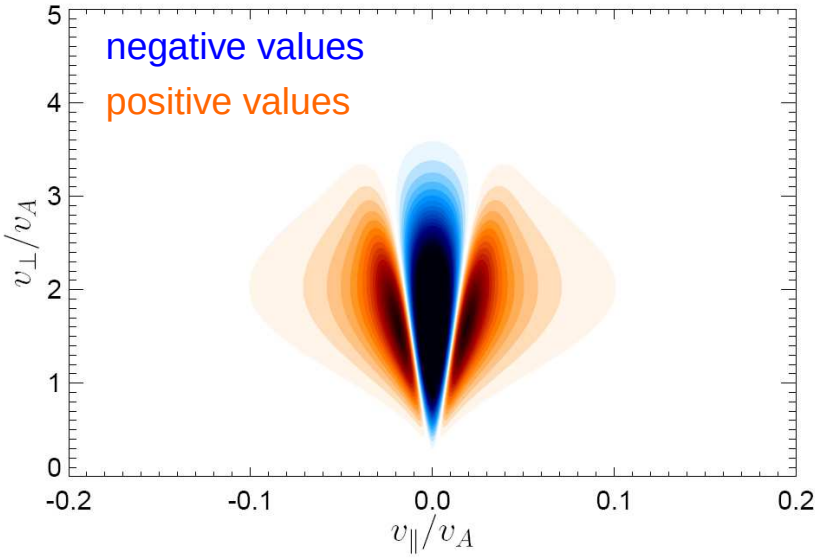

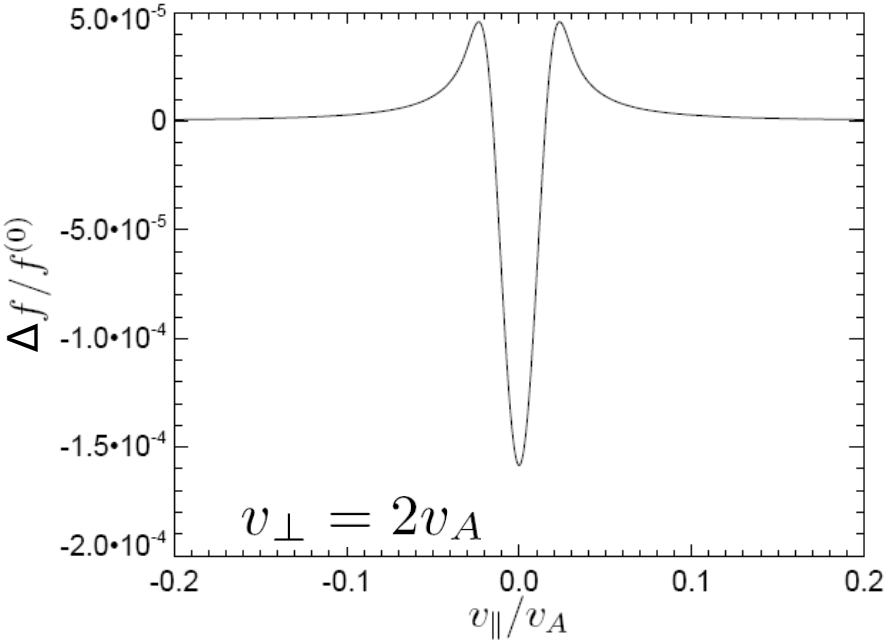

PIC simulation

t=2 10^3

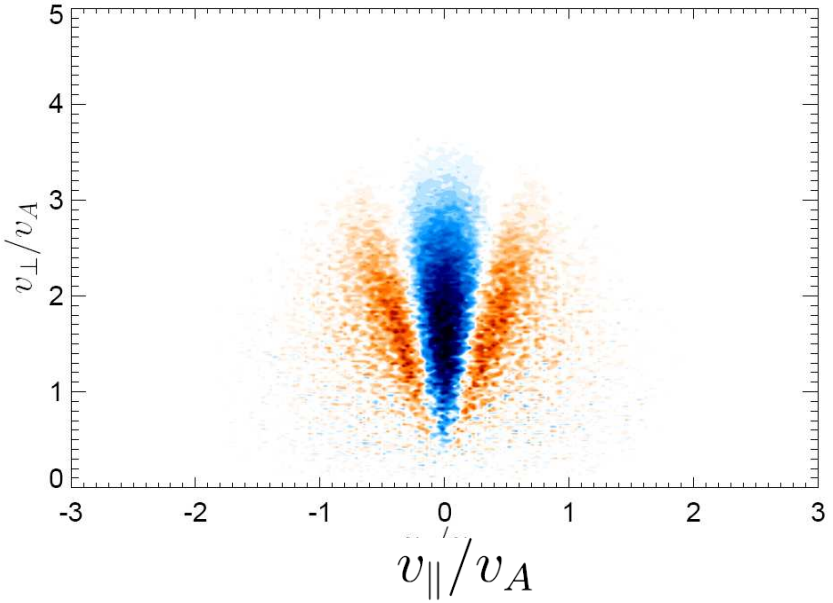

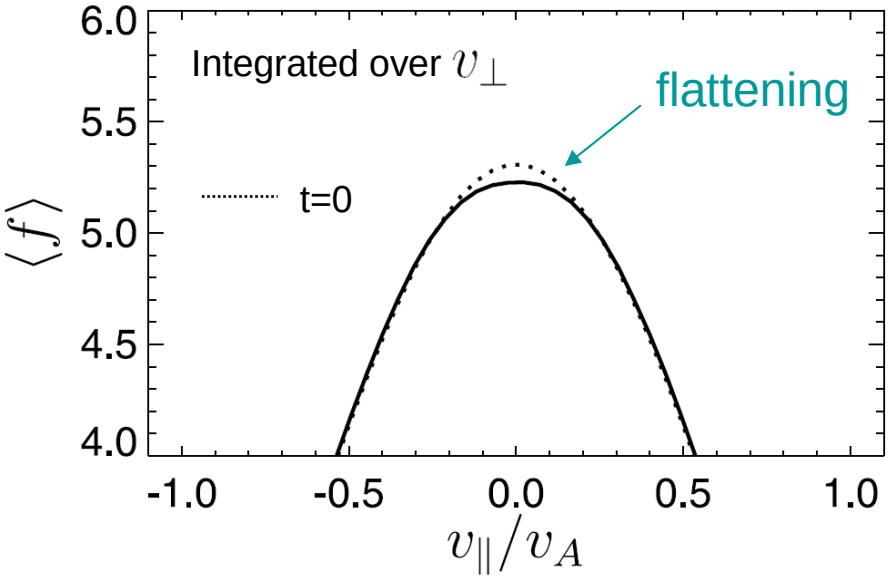

PIC simulation in an extended domain near threshold

Magnetic energy fluctuations

Gray scale plot of the magnetic fluctuations as a function of space and time.

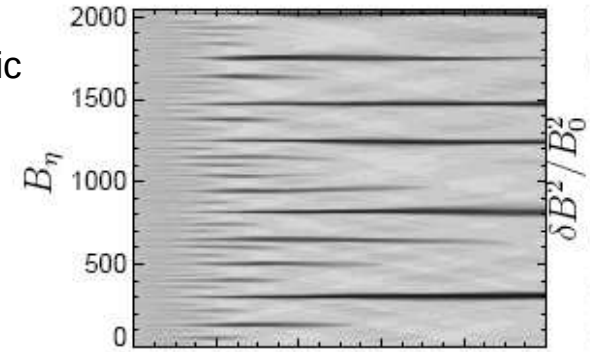

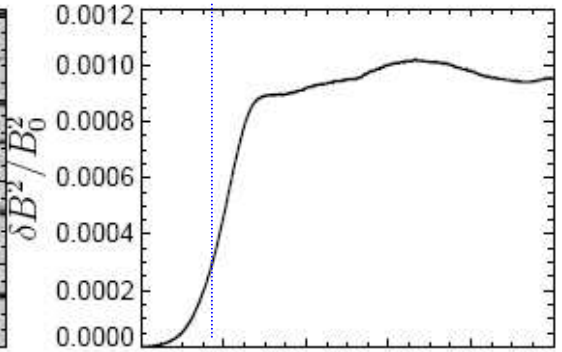

Bi-Maxwellian distance to threshold:

$$\Gamma^* = \beta_\perp \left(\frac{T_\perp}{T_\parallel} - 1 \right) - 1$$

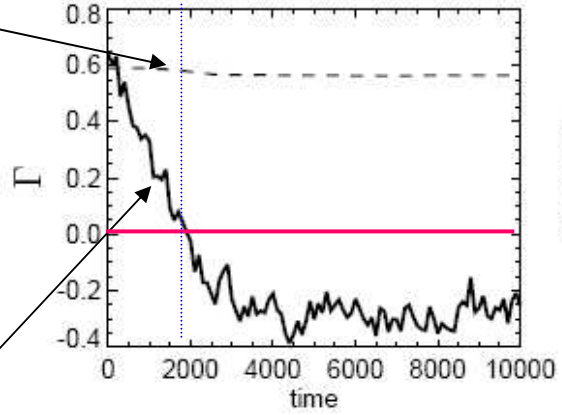

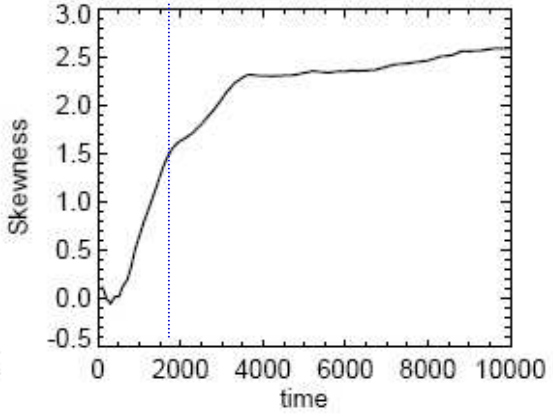

Instantaneous distance to threshold:

$$\Gamma = -\frac{m}{p_B} \int \frac{v_\perp^4}{4} \frac{\partial f}{\partial v_\parallel^2} d^3v - \beta_\perp - 1$$

Instantaneous distance to threshold reaches negative values, a signature that quasi-linear theory ceases to apply when coherent structures begin to form.

The instability continues to take place while $\Gamma < 0$, due to hydrodynamic-type nonlinear effects.

Positive skewness: magnetic humps.

No relaxation to marginal stability regime

3. Modeling the structure formation

A. Asymptotic expansion *(near a bi-Maxwellian equilibrium)*

Close to threshold, the linearly unstable mirror modes are confined to large scales.

Nonlinear dynamics amenable to a reductive perturbative expansion that isolates mirror modes *(Kuznetsov, Passot & Sulem, PRL, **98,** 235003 ,2007).*

At large scales, kinetic effects (Landau damping and finite Larmor radius corrections) are weak and contribute only linearly in the weakly nonlinear regime supposed to develop near threshold.

This argument is validated by a systematic reductive perturbative analysis performed on the Vlasov-Maxwell system *(Califano et al. JGR **113**, A08212, 2008)*.

For the sake of simplicity, assume cold electrons with negligible inertia.

Equation governing the proton velocity (derived from Vlasov equation)

$$\frac{du_p}{dt} + \frac{1}{\rho_p}\nabla \cdot \mathbf{p}_p - \frac{e}{m_p}(E + \frac{1}{c}u_p \times B) = 0$$

Assuming cold electrons with no inertia:

$$E = -\frac{1}{c}\left(u_p - \frac{j}{ne}\right) \times B \qquad \text{with} \qquad j = (c/4\pi)\nabla \times B$$

$$\mathbf{p}_p = p_\perp \mathbf{n} + p_{||}\boldsymbol{\tau} + \boldsymbol{\Pi} \qquad \text{with} \qquad \mathbf{n} = \mathbf{I} - \widehat{b} \otimes \widehat{b} \qquad \boldsymbol{\tau} = \widehat{b} \otimes \widehat{b} \qquad \widehat{b} = B/|B|$$

$$\rho\frac{du_p}{dt} = \nabla\left(p_\perp + \frac{|B|^2}{8\pi}\right) + \left(1 + \frac{4\pi}{|B|^2}(p_\perp - p_{||})\right)\frac{(B\cdot\nabla)B}{4\pi} - \widehat{b}\frac{|B|^2}{4\pi}(\widehat{b}\cdot\nabla)\left(1 + \frac{4\pi}{|B|^2}(p_\perp - p_{||})\right) + \nabla\cdot\boldsymbol{\Pi}$$

In order to address the asymptotic regime, we rescale the independent variables in the form $X = \sqrt{\varepsilon}x$, $Y = \sqrt{\varepsilon}y$, $Z = \varepsilon z$, $T = \varepsilon^2 t$, where ε measures the distance to threshold, and expand any field φ in the form

$$\varphi = \sum_{n=0} \varepsilon^{n/2}\varphi_{n/2}$$

Scalings of the space and time variables are suggested by the linear instability growth rate near threshold

$$\gamma = |k_z| v_{\text{th}||} \frac{\beta_{||}}{\sqrt{\pi}\beta_\perp}\left[\frac{\beta_\perp}{\beta_{||}} - 1 - \frac{1}{\beta_\perp} - \frac{k_z^2}{k_\perp^2\beta_\perp}\left(1 + \frac{\beta_\perp - \beta_{||}}{2}\right) - \frac{3}{4\beta_\perp}k_\perp^2\rho_L^2\right]$$

(ρ_L: ion Larmor radius)

In particular $B_\perp = \varepsilon^{3/2} B_\perp^{(3/2)} + \varepsilon^{5/2} B_\perp^{(5/2)} + \cdots$

$B_z = B_0 + \varepsilon B_z^{(1)} + \varepsilon^2 B_z^{(2)} + \cdots .$

E.B =0
cold electrons
without inertia

$E_\perp = \varepsilon^{5/2} E_\perp^{(5/2)} + \varepsilon^{7/2} E_\perp^{(7/2)} + \cdots$

$E_z = \varepsilon^5 E_z^{(5)} + \varepsilon^7 E_z^{(7)} \cdots .$

One shows that $\nabla_\perp \times B_\perp^{(3/2)} = 0$. By the divergenceless condition: $B_\perp^{(3/2)} = (-\Delta_\perp)^{-1} \nabla_\perp \partial_Z B_z^{(1)}$.

Defining $b_Z = B_Z^{(1)} + \varepsilon B_Z^{(2)}$ and $\overline{p}_\perp = p_\perp^{(1)} + \varepsilon p_\perp^{(2)}$,

the ion-velocity equation reduces to a **pressure balance equation**

$$\nabla \left[\overline{p}_\perp + \frac{B_0}{4\pi} b_z + \epsilon \frac{b_z^2}{8\pi} + \frac{2\varepsilon}{\beta_\perp} \left(1 + \frac{\beta_\perp - \beta_\parallel}{2} \right) p_\perp^{(0)} (\Delta_\perp)^{-1} \partial_{ZZ} b_z \right] + \epsilon \left(\nabla \cdot \Pi \right)_\perp^{(5/2)} = O(\varepsilon^2)$$

The perpendicular pressure and the gyroviscous force are to be calculated from Vlasov equation

For a biMaxwellian equlibrium:

$$\overline{p}_\perp = \beta_\perp \left(1 - \frac{\beta_\perp}{\beta_\parallel} \right) \frac{B_0 b_z}{4\pi} + \varepsilon \frac{\sqrt{\pi}}{v_{th\,\parallel}} \partial_T \left(- \mathcal{H}\, \partial_Z \right)^{-1} \frac{\beta_\perp^2}{\beta_\parallel} \frac{B_0 b_z}{4\pi}$$
$$- \epsilon p_\perp^{(0)} \left[\frac{9}{4\beta_\perp} r_L^2 \Delta_\perp \frac{b_z}{B_0} + \left(1 - 4\frac{p_\perp}{p_\parallel} + 3 \left(\frac{\beta_\perp}{\beta_\parallel} \right)^2 \left(\frac{b_z}{B_0} \right)^2 \right] \right]$$

$$\left(\nabla \cdot \Pi \right)_\perp^{(5/2)} = -\frac{3}{4} \left(1 - \frac{\beta_\perp}{\beta_\parallel} \right) p_\perp^{(0)} r_L^2 \Delta_\perp \nabla_\perp \left(\frac{b_Z}{B_0} \right)$$

In this near-threshold asymptotics,
- time derivative originates from Landau damping
- Landau damping and finite Larmor radius effects arise only linearly

r_L: ion Larmor radius

The vanishing of the contribution of zeroth order reproduces the instability threshold.

Dynamical equation obtained at the next order.

Dynamical equation *(assuming a bi-Maxwellian equilibrium):*

$$\partial_T\left(\frac{b_z}{B_0}\right) = \frac{v_{th\parallel}}{\sqrt{\pi}}\frac{\beta_\parallel}{\beta_\perp}\left(-\mathcal{H}\partial_Z\right)\left\{\frac{1}{\varepsilon}\left(\frac{\beta_\perp}{\beta_\parallel}-1-\frac{1}{\beta_\perp}\right)\left(\frac{b_z}{B_0}\right)+\frac{3}{4\beta_\perp}r_L^2\Delta_\perp\left(\frac{b_z}{B_0}\right)\right.$$
$$\left.-\frac{1}{\beta_\perp}\left(1+\frac{\beta_\perp-\beta_\parallel}{2}\right)\left(\Delta_\perp\right)^{-1}\partial_{ZZ}\left(\frac{b_z}{B_0}\right)-\frac{3}{2}\left(\frac{1+\beta_\perp}{\beta_\perp^2}\right)\left(\frac{b_z}{B_0}\right)^2\right\} = O(\epsilon).$$

After simple rescaling

$$\partial_\tau U = \left(-\mathcal{H}\partial_\xi\right)\left[\sigma U + \Delta_\perp U - \Delta_\perp^{-1}\partial_{\xi\xi}U - 3U^2\right]$$

Here, $\sigma = \pm 1$, depending on the positive or negative sign of the threshold parameter $\beta_\perp/\beta_\parallel - 1 - 1/\beta_\perp$.

When the spatial variation are limited to a direction making a fixed angle with the ambient field

$$\partial_T U = \widehat{K}_\Xi\left[\left(\sigma + \partial_{\Xi\Xi}\right)U - 3U^2\right]$$

$\hat{K}_Z = -\mathcal{H}\partial_Z$
whose Fourier transform is $|K_Z|$

where Ξ is the coordinate along the direction of variation.

Finite time blowup of the solution

When spatial variations are limited to a direction making a fixed angle with the ambient field:

$$\frac{\partial U}{\partial T} = \widehat{K}_{\Xi}\left[\left(\sigma + \frac{\partial^2}{\partial \Xi^2}\right) U - 3U^2\right]$$

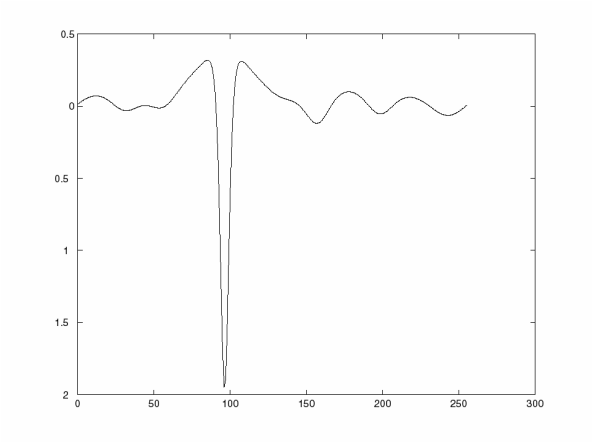

Solution profile near collapse

Integration above threshold (σ>1), with as initial conditions a sine function involving several wavelengths.

After an initial phase of linear instability, formation of a dominant magnetic hole.
After a while, solution blows up with a self-similar behavior.

Wave-particle resonance provides the trigger mechanism leading to the linear instability.

Hydrodynamic nonlinearities reinforce the instability, leading to collapse.

Linear FLR effects arrest the linear instability at small scales but cannot cope with hydrodynamic nonlinearities.

At the level of Vlasov-Maxwell eqs, the singularity is the signature of the formation of finite-amplitude structures, through a subcritical bifurcation that cannot be captured perturbatively.

Below threshold, this equation has the same stationary solutions as the KdV equation, but they are linearly unstable.

*Kuznetsov, Passot & Sulem, PRL **98**, 235003 (2007); JETP Letters, **86**, 637, 2007)*

Magnetic holes and not humps are obtained !

Reductive perturbative expansion

performed near bi-Maxwelian equilibrium,
retaining only linear kinetic effects,

predicts that the nonlinear development of the mirror instability leads to the formation of magnetic holes.

At least one of the two assumptions (bi-Maxwelian equilibrium,linear kinetic effects) is to be challenged.

B. Extension of the reductive perturbative expansion:

The reductive perturbative expansion near threshold can be extended to any (frozen) smooth equilibrium distribution function $f(v_\parallel^2, v_\perp)$ provided $\tilde{v} > 0$, $\tilde{r}^2 > 0$, and $\chi > 0$).

$$\partial_t b = \sqrt{\frac{2}{\pi}}\tilde{v}\,(-\mathcal{H}\partial_z)\left(\Gamma b + \frac{3}{2}\tilde{r}^2\Delta_\perp b - \chi\frac{\partial_z^2}{\Delta_\perp}b - \Lambda b^2\right) \qquad (\blacktriangle)$$

$b = \delta B_z(\boldsymbol{r},t)/B_0$ (normalized parallel magnetic perturbation)

$$\Lambda = \beta_\Lambda - 2\beta_\Gamma + \frac{\beta_\perp}{2} + \frac{1}{2}$$

neglecting the contribution of resonant particles to **Λ** in the case of a smooth distribution fonction

with $\beta_\Lambda = \dfrac{mn}{p_B}\displaystyle\int \frac{v_\perp^6}{8}\frac{\partial^2 f}{\partial (v_\parallel^2)^2}d^3v$

For a bi-Maxwellian distribution $\beta_\Lambda = 3/2\beta_\perp^3/\beta_\parallel^2$, thus **Λ** >0 and the model predicts formation of magnetic holes, while humps are observed in the simulations.

This suggests that the early-time QL dynamics affects the forthcoming formation of the structures.

We are thus led to modify eq.(▲) by assuming that **the coefficients** are not frozen at their initial values but **are evaluated from the instantaneous distribution function given by the QL diffusion equation**.

For consistency, the contribution of resonant particles are to be retained in the estimate of the nonlinear coupling constant.

$$\partial_t b = \frac{\sqrt{\frac{2}{\pi}}\tilde{v}}{1+2\frac{\tilde{v}}{v_\Lambda}b}\,(-\mathcal{H}\partial_z)\left(\Gamma b + \frac{3}{2}\tilde{r}^2\Delta_\perp b - \chi\frac{\partial_z^2}{\Delta_\perp}b - \Lambda b^2\right) \qquad (\blacktriangle\blacktriangle)$$

$$v_\Lambda^{-1} = \sqrt{2\pi}\frac{mn}{p_B}\int \frac{v_\perp^6}{8}\delta(v_\parallel)\frac{\partial^2 f}{(\partial v_\parallel^2)^2}d^3v$$

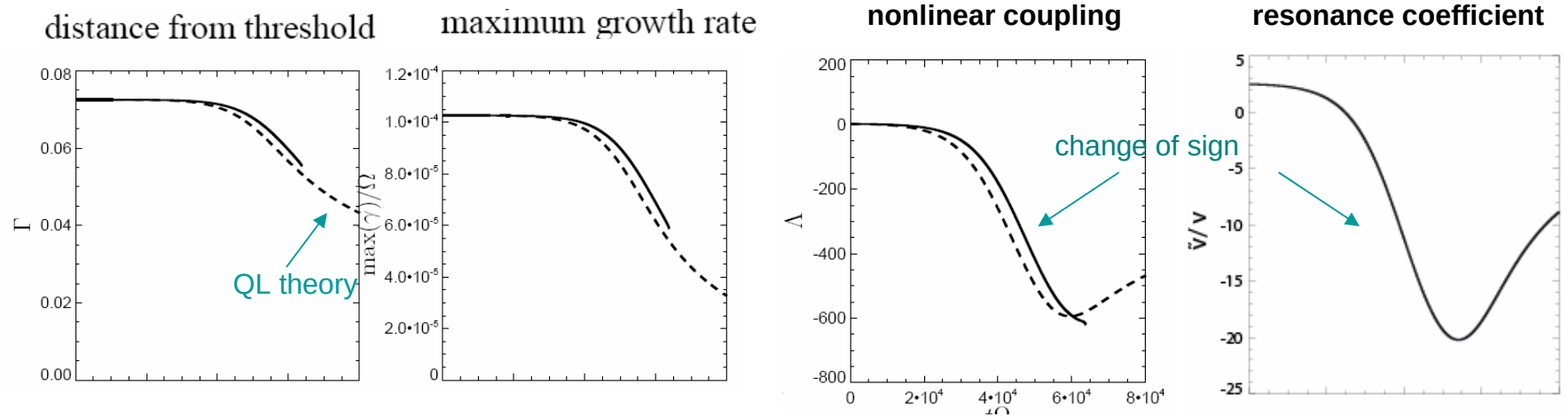

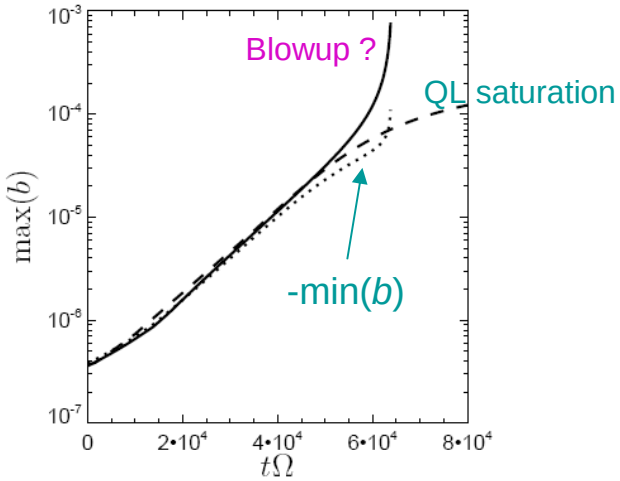

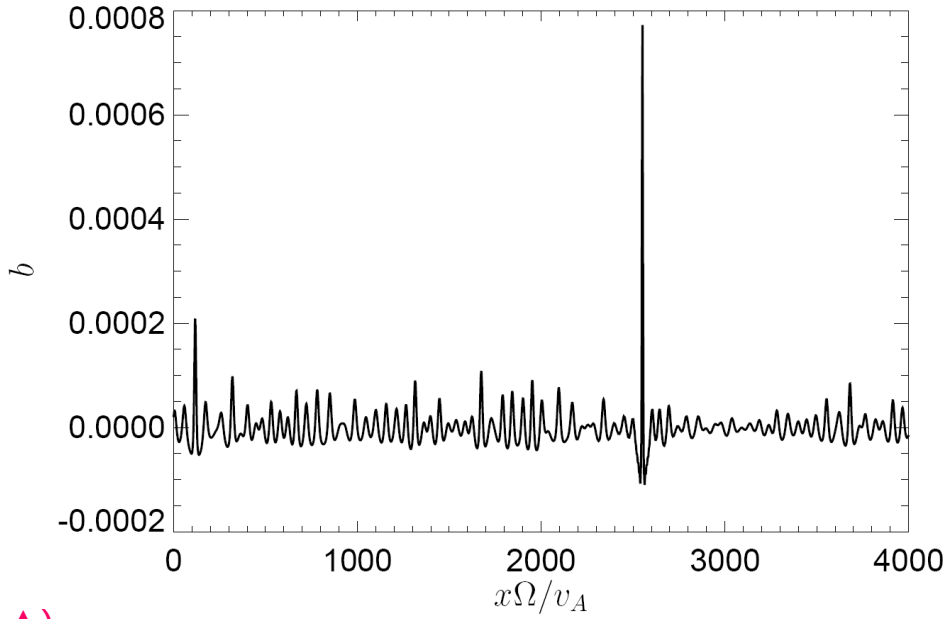

Results of the simulation of eq. (▲▲)
in 1D (in the most unstable direction)

Formation of magnetic humps

C. Properties and simulations of the model equation

Starting from a quasi-singular distribution function resulting from the QL evolution, a systematic expansion leads to a 1D equation which, after rescaling, reads:

$$\partial_t b = \frac{1}{1+s\alpha b}(-H\partial_\xi)\left(\sigma b + \mu\partial_{\xi\xi} b - 3sb^2\right)$$

where σ=+1 (supercritical) or -1 (subcritical)
s=+1 (near a Maxwellian distribution)
or s=-1 (due to QL flattening of distribution function)
The parameters α and μ are taken positive

The denominator is reminiscent (in a small amplitude expansion) of the *arctan* trapping correction suggested by Pokhotelov et al. (JGR 2008).
Note however that the physical mechanism is here different.

The denominator can arrest the collapse (for α and μ large enough) in the form of:
- magnetic hole solitons for s=+1
- magnetic hump solitons for s=-1

Saturated solutions in a supercritical regime

The numerical integration of the model equation (with μ=0.01, σ=1, s=-1, α=1) starting from a sine wave of amplitude 0.01 in a domain of size 2π leads to a quasi-stationary hump solution with a negative value of b in the background.

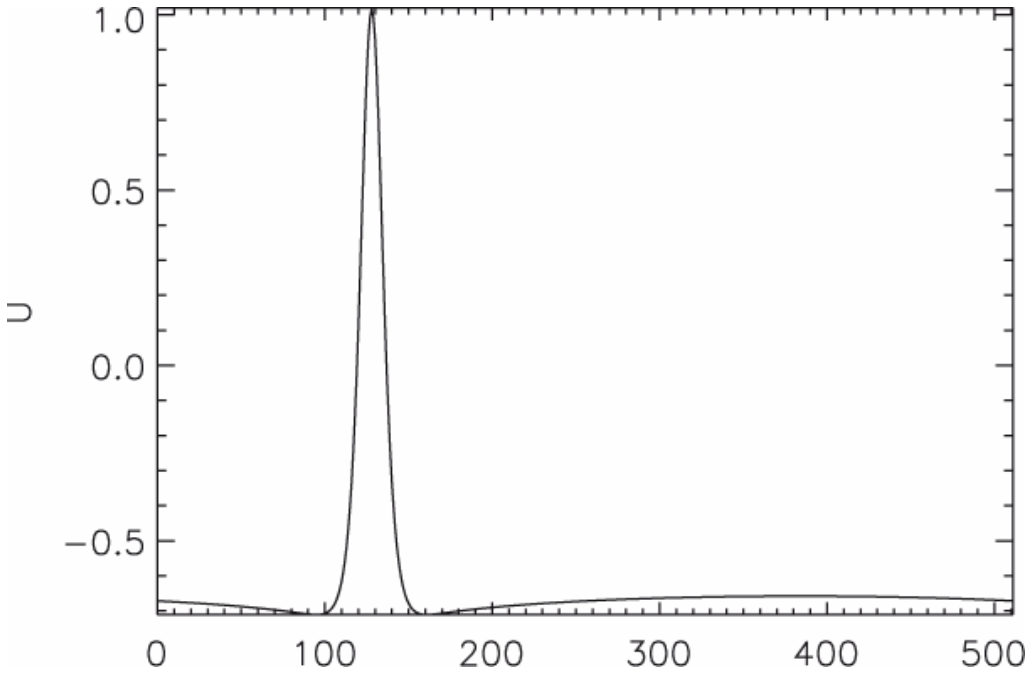

Note that the amplitude of the structures is prescribed by the strength of the early time QL resonance: larger amplitudes are obtained when these effects are small.

Saturation mechanism:

this problem is numerically (and mathematically) difficult
and is still under investigation. Extremely small time steps are required.

Existence and stability of the soliton profile:

As the nonlinear solution grows in amplitude, <b> gradually becomes negative;
at a certain point, the coefficient of the growth term for the fluctuations about <b>
becomes negative, putting the system in a situation similar to the subcritical regime.

The solution is then attracted to the negative of the KdV soliton
with an amplitude $b_{max}=1/\alpha$.
It is stable due to the presence of the denominator term.

For s=+1, hole solutions are obtained (change b into –b). They are physically relevant when QL effects are subdominant, even in a supercritical regime.

When starting with random initial conditions, which lead to a large number of humps, a coarsening phenomenon is observed.

Subcritical solutions

When σ=-1 with large initial data, no quasi-linear phase; the d.f. remains Gaussian (s=+1). The denominator correction (with α small) needs to be retained due to the large amplitudes.

Magnetic holes are thus obtained.

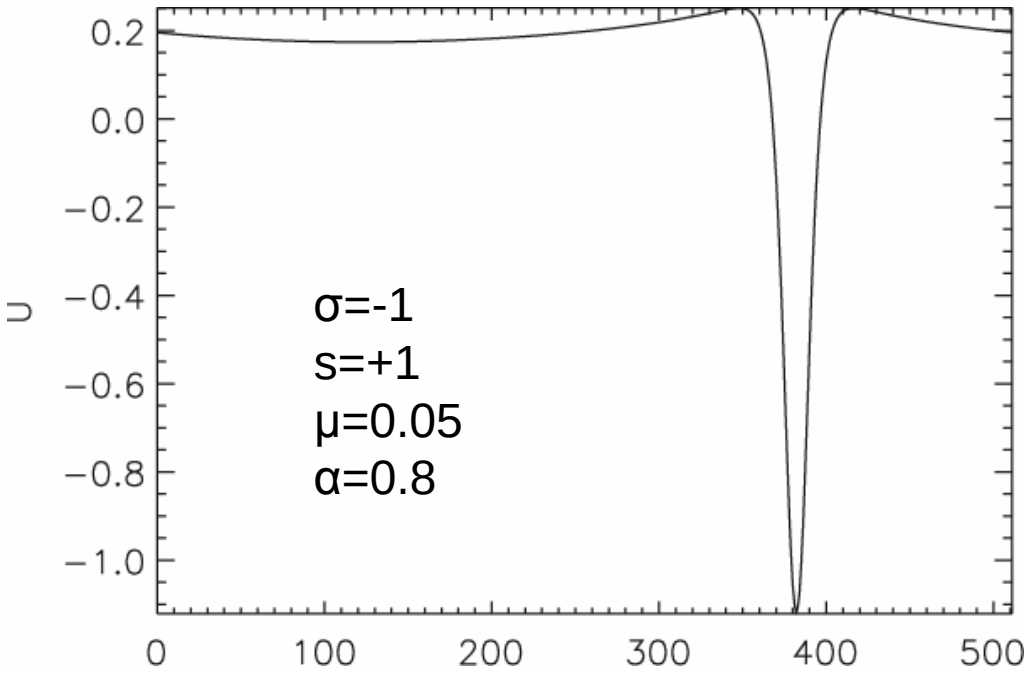

Formation of magnetic holes when starting with large initial perturbations

Vlasov simulation in a small domain

Domain size: 15x 2π c/ω_{pi}

Subcritical solutions (i.e. below threshold)

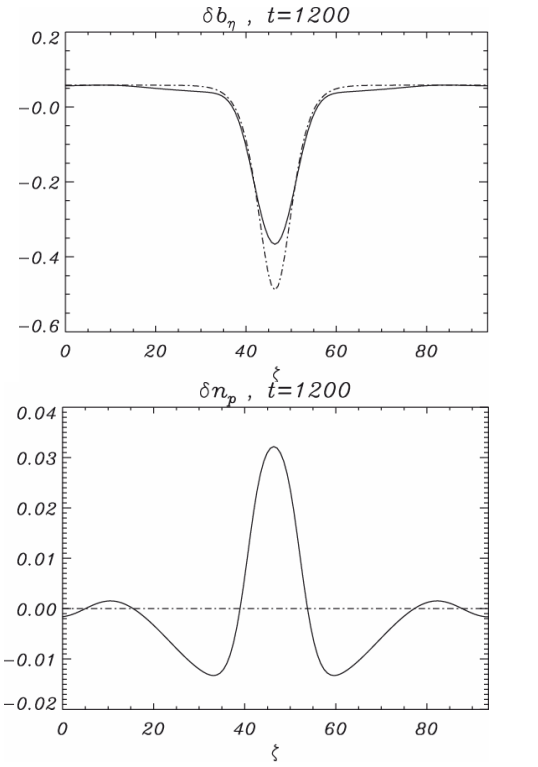

$$\beta_{\|} = 6, \quad \theta = 1.463, \quad T_\perp = T_{\|}$$

Large-amplitude magnetic holes
survive even far **below and above threshold**.

Magnetic humps do not survive

Solution above threshold.

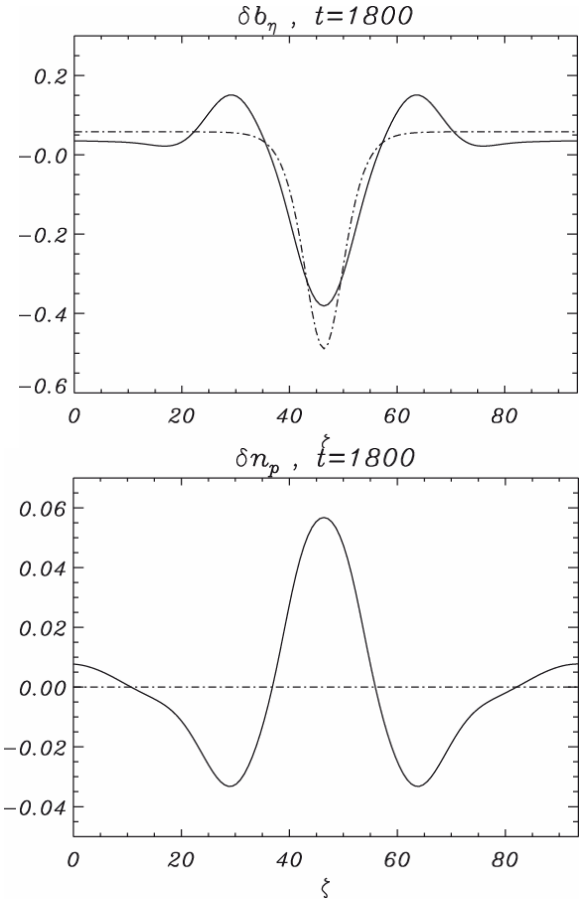

$\beta_{\|}$=6, $T_\perp/T_{\|}$=1.2 and θ=1.463

Simulation in a small computational domain

Using a PIC code

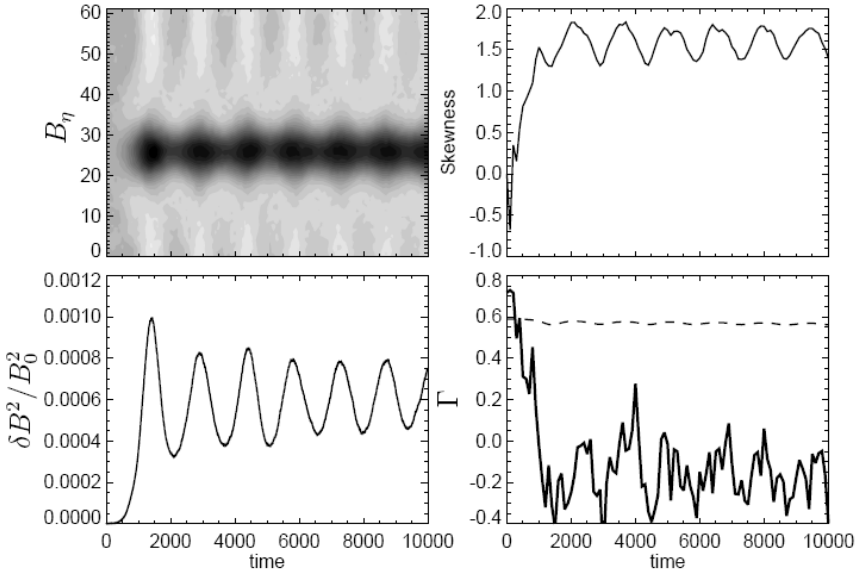

Oscillations of the magnetic energy fluctuations with a period consistent with the ion bounce time

$$\omega_{\rm tr}^2 = (1/2) v_{th_\perp}^2 k_\parallel^2 (\delta B/B_0)$$

Suggests that particle trapping is at the origin of oscillations.

The previous theory does not strictly apply to this situation, but still humps are formed!

Using an Eulerian code

Domain size (15x 2π c/ωpi)

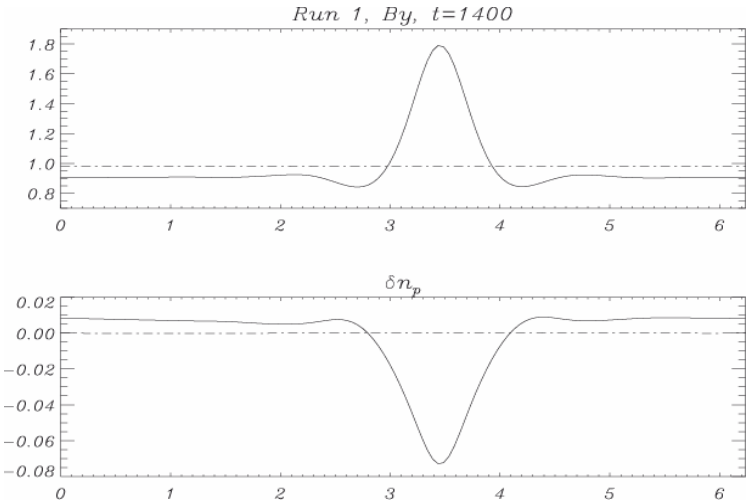

Magnetic hump (and density hole) resulting from the mirror instability, starting from noise.

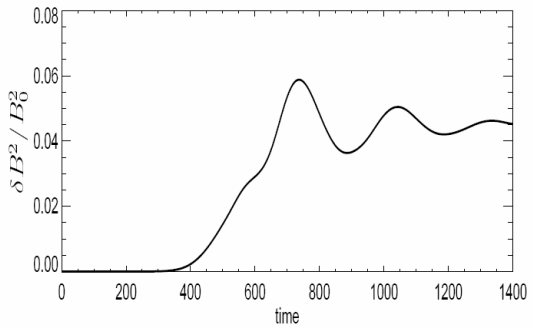

.

Amplitude oscillations, associated with particle trapping

Early understanding: saturation of mirror modes by relaxation to locally marginal stability

(Kivelson and Southwood 1996, Pantellini 1998).

Qualitative model where particles are divided in two groups that respond differently to the changing field.

Trapped particles with large pitch angle
Passing particles with small pitch angle $\alpha = \tan^{-1}(v_\perp / v_\parallel)$

In the rising field regions, trapped particles are excluded by the mirror force, leading to a decrease of the particle pressure (reduction of $\beta_\perp$) and evolution to marginal stability (with not important change in the particle energy).

In the well regions, no particle can be excluded.
Some trapped particles are cooled by loosing perpendicular energy (reduction of the temperature anisotropy).
Large reductions in the field are required in the wells in order to cool the trapped population enough to stabilize the system.

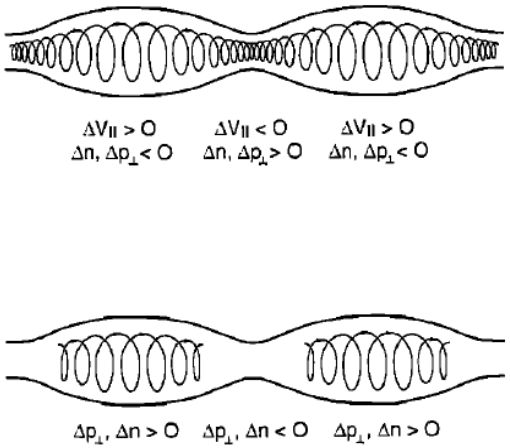

Figure 1. A schematic illustration of the distinction between the orbits of untrapped (upper panel) and trapped (lower panel) particles in a mirror geometry. Local velocity, density, and perpendicular pressure perturbations for adiabatic responses are characterized below each panel.

This model mostly predicts deep magnetic fields in conditions of marginal stability.

A recent quantitative model (Y. Istomin, O. Pokhotelov, M. Balikhin, PoP, **16**, 062905 2009) takes into account particle trapping and predicts the existence of soliton-like magnetic holes and nonlinear oscillatory solutions in the form of cnoidal waves.

All these approaches fail to explain the formation of magnetic humps

5. Summary

- Numerical integrations in a large domain of VM equations demonstrate the existence, when the mirror instability saturates, of an early phase described by the quasi-linear theory, followed by a regime where coherent structures form.

- In a small domain, no quasi-linear phase but significant oscillations due to particle trapping.

- **The structures resulting from the saturation of the mirror instabilty are magnetic humps, in small and large domains.**

- Stable solutions in the form of large-amplitude magnetic holes also exist both above and below threshold.

- Reductive perturbative expansion of VM eqs near threshold leads, for a bi-Maxwellian (and probably any smooth) equilibrium distribution function, to an equation with a finite-time singularity, signature of a **subcritical bifurcation**.

- An early quasi-linear phase introduces a boundary layer for the d.f. near $v_{//}=0$. As a result, the asymptotic equation leads to magnetic humps whose amplitude saturates at a level that depends on the strength of the quasi-linear resonance.

Refs: *Kuznetsov, Passot & Sulem, PRL 98, 235003 (2007); JETP Letters 86, 637 (2008)*
Califano, Hellinger, Kuznetsov, Passot, Sulem & Travnicek, JGR 113, A08219 (2008).
Hellinger, Kuznetsov, Passot, Sulem & Travnicek,GRL, 36, L06103, 2009.
Génot, Budbik, Hellinger, Passot, Belmont, Travnicek, Sulem, Lucek & Dandouras, Ann. Geophys. 27, 601 (2009).